Author Manuscript

Author Manuscript

Author Manuscript

Author Manuscript

HHS Public Access

Author manuscript

Cancer Res. Author manuscript; available in PMC 2017 January 15.

Published in final edited form as:

Cancer Res. 2016 January 15; 76(2): 472–479. doi:10.1158/0008-5472.CAN-15-2141.

Imaging, biodistribution, and dosimetry of radionuclide-labeled PD-L1 antibody in an immunocompetent mouse model of breast cancer

Anders Josefsson[*], **Jessie R. Nedrow**[*], **Sunju Park**, **Sangeeta Ray Banerjee**, **Andrew Rittenbach**, **Fabien Jammes**, **Benjamin Tsui**, and **George Sgouros**

Russell H. Morgan Department of Radiology & Radiological Science, Johns Hopkins University, School of Medicine, Baltimore, MD, USA

Abstract

The programmed cell death ligand 1 (PD-L1) participates in an immune checkpoint system involved in preventing autoimmunity. PD-L1 is expressed on tumor cells, tumor-associated macrophages, and other cells in the tumor microenvironment. Anti-PD-L1 antibodies are active against a variety of cancers, and combined anti-PD-L1 therapy with external beam radiotherapy has been shown to increase therapeutic efficacy. PD-L1 expression status is an important indicator of prognosis and therapy responsiveness, but methods to precisely capture the dynamics of PD-L1 expression in the tumor microenvironment are still limited. In this study, we developed a murine anti-PD-L1 antibody conjugated to the radioactive isotope Indium-111 (111In) for imaging and biodistribution studies in an immune-intact mouse model of breast cancer. The distribution of 111In-DTPA-anti-PD-L1 in tumors as well as the spleen, liver, thymus, heart, and lungs peaked 72 hours after injection. Co-injection of labeled and 100-fold unlabeled antibody significantly reduced spleen uptake at 24 hours, indicating that an excess of unlabeled antibody effectively blocked PD-L1 sites in the spleen, thus shifting the concentration of 111In-DTPA-anti-PD-L1 into the blood stream and potentially increasing tumor uptake. Clearance of 111In-DTPA-anti-PD-L1 from all organs occurred at 144 hours. Moreover, dosimetry calculations revealed that radionuclide-labeled anti-PD-L1 antibody yielded tolerable projected marrow doses, further supporting its use for radiopharmaceutical therapy. Taken together, these studies demonstrate the feasibility of using anti-PD-L1 antibody for radionuclide imaging and radioimmunotherapy, and highlight a new opportunity to optimize and monitor the efficacy of immune checkpoint inhibition therapy.

Keywords

Anti-PD-L1; antibodies; radiopharmaceutical therapy; immune checkpoint inhibitors; combination therapy

Corresponding author: Dr. George Sgouros, Russell H. Morgan Department of Radiology & Radiological Science, Johns Hopkins University School of Medicine, CRBII 4M.61, 1550 Orleans Street, Baltimore MD, 21231, USA, gsgouros@jhmi.edu.

[*]Authors contributed equally

Conflict of interest: None

Author Manuscript Author Manuscript Author Manuscript Author Manuscript

Introduction

The Programmed cell Death Ligand 1 (PD-L1), also referred to as B7-H1 (1) and designated as CD274 (2), is part of an immune checkpoint system that is essential for preventing autoimmunity (3). Recent work has shown that this system is co-opted by tumor cells to suppress anti-tumor immunity. PD-L1 is expressed on tumor cells, tumor associated macrophages (TAMs) and other cells in the tumor immune microenvironment that can inhibit $CD8^+$ T-cell effector function by its interaction with programmed cell death 1 (PD-1) (4). Anti-PD-L1 antibodies (Ab) have been developed, and are currently in clinical trial against a variety of cancers including breast cancer (5-7).

PD-L1 overexpression is associated with a poorer prognosis in a variety of cancers, but patients with PD-L1 overexpression typically have a stronger response to anti-PD-L1 therapy. For example, patients identified to overexpress PD-L1 in melanoma have a 39% response rate to anti-PD-L1 therapy, compared to a 13% response rate in patients with PD-L1 negative melanoma (8). Currently, immunohistochemistry (IHC) is utilized to evaluate PD-L1 expression in patients. PD-L1 is a dynamic biomarker, and its expression as determined by IHC is limited to a snapshot of the tumor environment (9). Accurately determining PD-L1 expression has the potential to identify patients who will best respond to anti-PD-L1 therapy, and monitoring changes in expression could provide information regarding treatment efficacy or potential toxicity. For example, high initial PD-L1 expression in the colon could warrant increased patient monitoring to avert irreversible colitis, one of the toxicities that has been observed in clinical trials.

The aims of this study were to develop and investigate a targeted anti-PD-L1 radiopharmaceutical for use as a molecular imaging agent. The resulting compound ^{111}In-DTPA-anti-PD-L1 was evaluated in an immune-competent transgenic mouse model of breast carcinoma (10) to reflect the role of PD-L1 in the immune system. Furthermore, through dosimetry we evaluated the potential of this agent to serve as a targeted radiopharmaceutical for PD-L1 targeted radionuclide therapy.

Material and methods

Reagents—All chemicals were purchased from Sigma-Aldrich Chemical Co. (St. Louis, MO, USA) or Thermo Fisher Scientific (Pittsburgh, PA, USA), unless otherwise specified. Aqueous solutions were prepared using ultrapure water (resistivity, 18 MΩ·cm) treated with Chelex resin purchased from Bio-Rad Laboratories, Inc. (Berkeley, CA, USA). p-SCN-Bn-DTPA was purchased from Macrocyclics, Inc. (Dallas, TX, USA). [^{111}In]$InCl_3$ was purchased from MDS Nordion (Vancouver, BC, Canada). The anti-murine PD-L1-reactive antibody used is described in reference (11).

Radiolabeling of DTPA-anti-PD-L1 antibodies with ^{111}In—The anti-PD-L1 Ab was conjugated to *N*-[2-amino-3-(*p*-isothiocyanatophenyl)propyl]-*trans*-cyclohexane-1,2-diamine-*N*,*N*′,*N*′,*N*″,*N*″-pentaacetic acid (SCN-CHX-A″-DTPA) using previously described standard methods yielding DTPA-anti-PD-L1 (12,13). Indium-111 ([^{111}In]$InCl_3$) (37-74 MBq) was added to an acid washed 1.5 mL eppendorf tube containing 0.25 mL of 0.2 M

Author Manuscript Author Manuscript Author Manuscript Author Manuscript

HCl and 0.03 mL of 3 M NH_4OAc, pH=7. After a minute, 0.2 mg of DTPA-anti-PD-L1 Ab was added to the mixture. The mixture was allowed to set at room temperature for 45-60 min then transferred to an Amicon Ultra 10 K centrifugal filter device. PBS was added and the device was centrifuged for 15 min at 3000 rpm to remove free [^{111}In]$InCl_3$ (1×). Radiochemical purity of >98% was determined by radio TLC, and the protein concentration was determined by Nanodrop (Wilmington, DE, USA).

In vitro studies

Cell lines—The NT2.5 cell line was established from spontaneous mammary tumors in female *neu*-N mice (14,15). A frozen stock of these cells was obtained from Dr. Elisabeth Jaffe's lab at Johns Hopkins University. The PD-L1 expression of NT2.5 cells was compared with 4T1, a murine mammary carcinoma cell line, and HBL100, a human breast cancer cell line, both provided by Dr. Saraswati Sukumar at Johns Hopkins University. The EL4.murineB7H1 (EL4), a murine lymphoma cell line, transfected to express murine PD-L1, served as a positive control (16). Frozen EL4 cells were obtained from Amplimmune, Inc. (Gaithersburg MD). 4T1 and HBL100 cell lines obtained from Sukumar Lab in 2014 were purchased from ATCC (authenticated using STR profile analysis). NT2.5 and EL4 Cell lines obtained from the Jaffee and Amplimmune in 2014 were not authenticated by the Sgouros lab. Cells were cultured for a maximum of 4 weeks before thawing fresh, early passage cells. HER2 status in the NT2.5 cell line was confirmed by Western blot analysis and Real-Time RT-qPCR. All cells were confirmed to be Mycoplasma negative (Hoechst stain and PCR; tested in 2014). NT2.5 cells were grown in RPMI1640 media with 20% fetal bovine serum (FBS) + 1.2% HEPES + 1% L-glutamine + 1% non-essential amino acids (NEAA) + 1% sodium pyruvate + 0.2% insulin + 0.02% gentamycin. 4T1 cells were grown in RPMI 1640 media supplemented with 10% FBS. EL4 cells were grown in DMEM media + 10% horse serum + 1% Penicillin/Streptomycin (PS). HBL100 cells were grown in DMEM media + 10% FBS + 1% PS. All cell lines were incubated at 37 °C in 5% CO_2. Cell incubation with interferon-gamma (IFN-γ) was performed by removing the growth medium and incubating the cells overnight in media with 1% serum and 200 ng/ml recombinant mouse INF-γ (EMD Millipore, Temecula, CA, USA).

Real-Time RT-qPCR—Total RNA was extracted with Trizol reagent (Invitrogen, Grand Island, NY, USA), and cDNA was synthesized from total RNA (2 μg) using an M-MLV Reverse Transcriptase (Promega, Madison, WI, USA). Aliquots of cDNA were used as templates for real-time RT-qPCR procedure using a PD-L1 specific primer (Forward: 5′ GCTTCTCAATGTGACCAGCA 3′, Reverse: 5′ GAGGAGGACCGTGGACACTA 3′). Relative quantities of mRNA expression were analyzed using real-time PCR (Applied Biosystem 7500 Real-Time PCR system, Applied Biosystems, Grand Island, NY, USA). The Maxima SYBR Green/ROX Master Mix (Fermentas, Pittsburgh, PA, USA) was used according to the manufacturer's instruction.

Flow cytometry—Cell lines were cultured for 24 hrs in the presence or absence of IFN-γ. Cells were trypsinized, washed with PBS solution, and blocked with PBS containing 10% FBS. 2×10^5 cells were incubated with anti-mouse B7-H1 (CD274)-PE clone M1H5 (ebioscience, San Diego, CA, USA) for 30 min at 4 °C. After repeated washing, cells were

Author Manuscript Author Manuscript Author Manuscript Author Manuscript

resuspended in 500 μl of PBS and analyzed on a FACS flow cytometer (BD Biosciences, San Jose, CA, USA).

Immunohistochemistry—IHC staining was performed on 8 μm thick cryo-sectioned tissue samples of the NT2.5 tumor, spleen, thymus, liver and kidneys. The tissue samples were fixed by acetone (4 °C) for 10 min. Endogenous peroxide activity was quenched by 10 min incubation in 3% H_2O_2 and non-specific binding was blocked with serum. The dilution of 1:50 of primary Ab (Anti-PD-L1, Abcam, Cambridge, MA, USA) was incubated at room temperature (16 hrs). Diluted biotinylated anti-rabbit IgG (Vectastain kit, Vector Laboratories, Burlingame, CA, USA) was added to the tissue samples and incubated for 30 min. Vectastain ABC reagent and DAB was used for staining color development, and the counterstaining was performed with hematoxylin solution.

Binding assay—Cell experiments were performed to determine the binding affinity of ^{111}In-DTPA-anti-PD-L1 in NT2.5 cells. Cells were seeded in 24-well plates (50,000-100,000 cells) 36 hrs prior to the experiment. INF-γ (400 ng) was added to each well 24 hrs prior to the experiment, to induce PD-L1 expression. Before the experiment, cells were washed (1×) with PBS (1 mL), and 0.5 mL growth media (RPMI 1640 with 0.1% PS and 10% FBS) was added to each well. To determine non-specific binding, 5 μg of anti-PD-L1 was added to half of the wells as a cold block 30 min prior to ^{111}In-DTPA-anti-PD-L1. ^{111}In-DTPA-anti-PD-L1 was added to all the wells in increasing concentrations (1.0–25 nM). The samples were incubated for 2.5 hrs on ice. After incubation, the radioactive media was removed. Cell pellets were rinsed twice with PBS (1 mL) and dissolved in 0.5% SDS solution. The radioactivity in each fraction was measured in a gamma well counter (Perkin-Elmer 2470 WIZARD^2® Automatic Gamma Counter, Waltham, MA, USA). The protein content of each cell lysate sample was determined (BCA Protein Assay Kit, Pierce). The measured radioactivity associated with the cells was normalized to the amount of cell protein present (cpm/mg protein). The K_d and B_{max} were calculated using PRISM 5 (Graphpad; La Jolla, CA).

In vivo studies

Animals—Mouse imaging and biodistribution studies were performed using the rat HER-2/*neu* expressing mouse mammary cell line, NT2.5 in *neu*-N transgenic (17) healthy female mice, 8 to 12 weeks old, both obtained courtesy of Dr. Elizabeth Jaffee at Johns Hopkins University. All animal studies were approved by the Animal Care and Use Committee of the Johns Hopkins University, School of Medicine. All mice were subcutaneously (s.c) injected in the left flank with 10^5 cells in 50 μl matrigel. In addition, mice used for SPECT imaging were also injected s.c. with 10^6 cells/50 μl matrigel in the right flank. All injections were done 3 weeks prior to experiments.

SPECT imaging of ^{111}In labeled anti-PD-L1 antibodies in tumor bearing neu-N mice—Tumor bearing healthy female *neu*-N transgenic mice were each injected intravenously (i.v.) with 7.4 MBq ^{111}In-DTPA-anti-PD-L1. The mice (n=3) were imaged at 1, 24 and 72 hrs post-injection (p.i.) with the VECTor^4 SPECT imaging system (MILabs, Utrecht, The Netherlands) using a general purpose mouse collimator, with 0.6 mm pinholes

Author Manuscript Author Manuscript Author Manuscript Author Manuscript

and imaging resolution of 0.4 mm.. Images were acquired for 60 min at the 1 and 24 hrs time points, and for 90 min at the 72 hrs time point. Images were reconstructed with voxel side length 0.2 mm using POS-EM (18), a vendor supplied iterative algorithm. After reconstruction, a 3D-Gaussian filter with a 0.6 mm FWHM was applied to each image.

Biodistribution of ^{111}In labeled anti-PD-L1 antibodies in tumor bearing neu-N mice—Biodistribution experiments were conducted as previously described with minor modifications (19). Briefly, healthy NT2.5 tumor-bearing female *neu*-N transgenic mice (n=4/time point) were injected i.v. with ^{111}In-DTPA-anti-PD-L1 (∼0.93 MBq, 8.4 μg). At 1, 24, 72, and 144 hrs p.i. the mice were sacrificed. The blood, heart, lungs, liver, kidneys, spleen, stomach (with content), intestine (with content), femur, thymus, muscle, and tumors were harvested, weighed, and measured in a gamma well counter. In addition, competitive blocking studies were performed at 24 hrs p.i. The mice were co-injected with ^{111}In-DTPA-anti-PD-L1 and unlabeled (cold) anti-PD-L1 Ab (30× and 100×). The percent injected dose per gram (%ID/g) was calculated by comparison to a weighed, diluted standard.

Normal tissue and tumor dosimetry—Normal tissue and tumor absorbed dose (AD) calculations were performed for ^{177}Lu and ^{90}Y (candidates radionuclides for therapy), and ^{111}In (used in diagnostic imaging). The organ activity concentrations obtained from the murine biodistribution studies using ^{111}In-labeled Ab ($[\%\ ID/g]_M$) were translated to human whole-organ percent of injected dose ($[\%\ ID/organ]_H$) based on the principle that the organ to whole-body activity concentration ratio of a radiopharmaceuticals in mice would equal that in humans. This principle is implemented in the following expression:

$$[\%\ ID/organ]_H = [\%\ ID/g]_M \cdot OW_H \cdot \frac{TBW_M}{TBW_H} \quad (1)$$

Where OW_H is the human organ weight, TBW_M is the average total body weight of the mice (TBW_M = 25 g), and TBW_H the average total body weight for an adult male (TBW_H = 73.7 kg) (20,21). The activity concentration in human red marrow was estimated using a previously described blood-based method (22) wherein the activity concentration obtained at each time-point in the murine biodistribution studies (A_{BL}) was related to the red marrow activity concentration in a human (A_{RM}) using the following expression:

$$A_{RM} = A_{BL} \cdot \frac{RMCEFF}{(1 - HCT)} \quad (2)$$

RMECFF is the red marrow extracellular fluid fraction (*RMECFF* = 0.19), and *HCT* is the volume fraction of red blood cells in blood (*HCT* = 0.47) in humans.

Whole-organ time-integrated activity coefficients (TIACs) were calculated for ^{177}Lu and ^{90}Y by applying the half-life of these two radionuclides to the decay corrected pharmacokinetics obtained using ^{111}In. The resulting radioactivity concentrations versus time curves for each organ were integrated using a hybrid numerical integration/analytical integration method. If the data could be fit to a one or two exponential expression, then the

Author Manuscript Author Manuscript Author Manuscript Author Manuscript

curves were integrated analytically from zero to infinity. Alternatively numerical integration was performed over the measured data and the last two time-points were used to derive a single exponential function that was analytically integrated beyond the last measurement. The MIRD Committee methodology (23,24) as implemented in OLINDA/EXM (25) was used to calculate organ AD. Tumor absorbed dose was estimated using the sphere module in OLINDA/EXM to calculate the AD to a sphere from photon and electron emissions originating within the sphere.

Statistical analysis

Statistical analysis was performed using the software, GraphPad (La Jolla, CA USA). All data are presented as the mean value ± standard deviation. Groups were compared using two tailed student *t*-test, and p-values were considered significant if ≤ 0.05.

Results

Radiochemistry—The ^{111}In-DTPA-anti-PD-L1 conjugate was radiolabeled in 45-60 min at room temperature in ammonium acetate buffer at a specific activity of 110-122 MBq/μg with >98% radiochemical purity following purification.

In vitro studies

Real-Time RT-qPCR—To examine the level of PD-L1 mRNA in the breast cancer cell lines treated with IFN-γ, we performed Real-Time RT-qPCR for the cell lines 4T1, NT2.5, and HBL100 using designed human or mouse PD-L1 specific primers. In addition, EL4 was evaluated to serve as a positive control. The results showed that PD-L1 mRNA levels were significantly increased in the IFN-γ treated murine cell lines, 4T1 and NT2.5, but not HBL100, a human breast cancer cell line (Figure 1). Interestingly, PD-L1 mRNA in HER2 positive NT2.5 cells was 4.5 times higher than in the triple negative 4T1 cells.

Flow cytometry—Cell-surface expression of PD-L1 with and without IFN-γ treatment was evaluated by flow cytometry (Figure 2A-D). PD-L1 expression on the positive control line, EL4, was not significantly increased with IFN-γ. PD-L1 expression on 4T1 cells increased 2.7-fold with INF-γ incubation. The highest, 7.5-fold, increase in PD-L1 expression was obtained with NT2.5 cells.

Immunohistochemistry—IHC was performed on tissue samples from NT2.5-tumor bearing *neu*-N mice (Figure 3). The NT2.5 tumors showed high expression of PD-L1 in the cytoplasm and on the membranes. The spleen showed high expression of PD-L1 on the membranes, the kidneys showed low expression, the thymus showed low expression, and the liver had very low to no expression of PD-L1.

Binding assay—Saturation binding assay shows that ^{111}In-DTPA-anti-PD-L1 binds with high affinity to PD-L1 with a K_d of 8.3±3.2 nM and a B_{max} of 65.4±10.1 fmol/mg (approximately 1.4×10^4 sites/cell). It should be noted that without INF-γ in the binding assay, NT2.5 cells do not show binding of ^{111}In-DTPA-anti-PD-L1.

Author Manuscript Author Manuscript Author Manuscript Author Manuscript

In vivo studies

SPECT imaging of ^{111}In labeled anti-PD-L1 antibodies in tumor bearing neu-N mice—Whole body coronal SPECT image slices show the distribution of ^{111}In-DTPA-anti-PD-L1 at 1, 24 and 72 hrs p.i. (Figure 4). At 1 h p.i. signal intensity was highest in the liver, spleen and thymus, but was also observed in the region of the spinal column. The signal intensity within the spinal column likely reflects the high concentration of ^{111}In-DTPA-anti-PD-L1 in the circulation. At 24 and 72 hrs p.i. clearance of ^{111}In-DTPA-anti-PD-L1 from non-target tissues including the blood and accumulation in PD-L1 rich sites allowed visualization of the isografts. Relative to 1 hr, liver intensity was reduced while signal intensity in the spleen and thymus persisted.

Biodistribution of ^{111}In-DTPA-anti-PD-L1 antibodies in tumor bearing neu-N mice—The distribution of ^{111}In-DTPA-anti-PD-L1 in NT2.5 tumor-bearing *neu*-N mice was obtained by *ex vivo* counting of tissues collected from mice sacrificed at different time points p.i. (Figure 5A). The results obtained from these studies were generally consistent with the imaging observations of Figure 4. At 1 hr p.i., ^{111}In-DTPA-anti-PD-L1 was mainly in the blood (28.7±15.6 %ID/g) and spleen (24.8±6.3 %ID/g). Tumor concentration at this time was 3.9±2.3 %ID/g. By 24 hrs blood concentration decreased to 12.6±2.2. ^{111}In-DTPA-anti-PD-L1 cleared from the blood with a 40.8 hr biological half-life. The imaging probe's concentration in tumor, spleen, liver, thymus, heart and lung increased to 29.5±7.4, 63.9±12.2, 21.9±6.0, 11.8±2.0, 6.2±1.9, and 9.6±2.7 %ID/g, respectively. At 72 hrs accumulation of ^{111}In-DTPA-anti-PD-L1 peaked in the tumor at 56.5±16.7 %ID/g with moderate tumor to muscle/blood ratios (23±8, 4±1). The spleen (102.4±12.8 %ID/g), liver (29.7±5.8 %ID/g), thymus (31.0±17.6 %ID/g), heart (8.7±1.5 %ID/g), and lung (12.1±2.0 %ID/g) also had the highest accumulation at 72 hrs. Accumulation in other organs at this time was low, with uptake decreasing or remaining constant. Clearance of ^{111}In-DTPA-anti-PD-L1 from all organs was seen at 144 hrs. At this time the concentration in tumor (21.1±11.2 %ID/g) was significantly greater than other organs, except the spleen (63.5±25.4 %ID/g), liver (14.9±4.2 %ID/g), and thymus (16.8±16.2 %ID/g).

In the presence of excess unlabeled anti-PD-L1 Ab, the 24-hr distribution of ^{111}In-DTPA-anti-PD-L1 was significantly altered (Figure 5B). Co-injection of the labeled Ab with 30 or 100-fold unlabeled Ab reduced the 24-hr spleen uptake to 16.2±1.8 %ID/g ($p \leq 0.0002$, relative to unblocked) and 10.7±5.0 %ID/g, ($p \leq 0.0002$, relative to unblocked), respectively; the concentration in blood increased to 45.2±5.5 ($p \leq 0.0001$) and 43.0±13.0 ($p \leq 0.004$) %ID/g, respectively. ^{111}In-DTPA-anti-PD-L1 concentration in the tumor at 30 and 100 times the blocking dose was 21.2±3.8 ($p \leq 0.09$, relative to unblocked) and 17.6±5.4 %ID/g ($p \leq 0.04$, relative to unblocked), respectively. The 24 hrs uptake in the thymus was not blocked.

Normal organ and tumor dosimetry—AD calculations for selected tissues are listed in Table 1. As expected from the biodistribution data, the highest AD for each radionuclide is to the spleen. ^{90}Y-labeled anti-PD-L1 Ab would deliver 8.2mGy/MBq while ^{177}Lu would deliver 2.5 mGy/MBq to the spleen corresponding tumor ADs are 3.0 and 1.1 mGy/MBq, respectively. The tumor to red marrow AD ratio is about 10 for both therapeutic

Author Manuscript Author Manuscript Author Manuscript Author Manuscript

radionuclides. The thymus had high ADs of 0.7 and 2.2 mGy/Mbq, and the liver's ADs were 0.8 and 2.7 mGy/Mbq for ^{177}Lu and ^{90}Y-Ab, respectively.

Discussion

Antibodies against PD-L1 have shown great promise in patients with a variety of cancers (5), as part of a novel immune checkpoint blockade treatment strategy (3). Patients with PD-L1 overexpression have typically demonstrated a greater response to anti-PD-L1 Ab therapy compared to patients with low or negative PD-L1 expression. However, mixed responses to anti PD-L1 therapy highlight the need to develop methods that better predict whether a patient will respond to anti PD-L1 therapy (8). Furthermore, the response to therapy targeting the PD-L1/PD-1 axis has been shown to improve when combined with external-beam radiation therapy in preclinical studies (26,27). In this work we examined the feasibility of using anti-PD-L1 Ab for radionuclide imaging and radioimmunotherapy.

PD-L1 is a dynamic biomarker with its expression varying in response to the immune system. Our *in vitro* studies helped highlight the dynamic nature of PD-L1 expression and its response to immune signals, such as IFN-γ. IFN-γ has been reported to induce PD-L1 expression in a variety of cells (28,29). The real-time RT-qPCR and flow cytometry results confirm that the PD-L1 expression in the murine-derived mammary carcinoma cells is highly dependent on inflammatory signaling. In the presence of IFN-γ, the highest PD-L1 up-regulation at both the mRNA and cell surface levels was seen in the endogenously derived NT2.5 tumor cell line. IHC confirmed the high expression of PD-L1 in NT2.5 tumors. In addition, IHC demonstrated high PD-L1 expression in the spleen, while expression in liver, kidneys, and thymus was substantially lower in the *neu*-N model.

The *in vivo* imaging and biodistribution data provided in this work illustrate a number of principles that could be used to guide and potentially optimize immune checkpoint therapy. Whole-body imaging helps identify cross-reactive normal organs. Whole-body SPECT images of ^{111}In-DTPA-anti-PD-L1 showed high signal intensity in the PD-L1 positive isografts and in potentially cross-reactive organs such as the spleen and thymus. The biodistribution data supported the SPECT imaging and demonstrated that tumor, spleen, and thymus had the highest uptake at 72 hrs p.i. The imaging and biodistribution results were generally consistent with IHC staining. However, the thymus demonstrated high uptake of ^{111}In-DTPA-anti-PD-L1 Ab, but was identified by IHC to have medium to low expression of PD-L1. Although PD-L1 expression in the thymus and spleen has been previously noted (30), the impact of such cross-reactivity on overall kinetics could not be appreciated without the *in vivo* studies presented here.

Recently, Heskamp *et al.* used a human tumor (MB231) xenograft in an athymic mouse model to demonstrate that a human PD-L1 Ab can be imaged with minimal cross-reactivity to other normal organs (31), the animal model used lacked a thymus and, correspondingly, the ability to produce T cells, a key component in the PD-1/PD-L1 axis. In an immunologically intact model, using an Ab against murine PD-L1, we show substantial uptake in the spleen and thymus, which was not demonstrated in the immune deficient mouse model. Furthermore, the mouse model used in our experiments demonstrated that the

Author Manuscript Author Manuscript Author Manuscript Author Manuscript

spleen is a sink for ^{111}In-DTPA-PD-L1, confirmed by the co-administration of ^{111}In-DTPA-PD-L1 and excess unlabeled Ab. The co-administration of excess unlabeled anti-PD-L1 Ab effectively and dramatically blocked PD-L1 sites in the spleen, shifting the concentration of ^{111}In-DTPA-PD-L1 into the blood. In addition, reduced blocking was seen in the tumor but not to the extent seen in the spleen. Surprisingly, significant blocking was not observed in the thymus, suggesting a large pool of PD-L1 positive cells in this tissue. It is also possible that the F_c portion of the antibody is binding to sites on the thymus. These results suggest that a pre-dosing strategy with unlabeled Ab has the potential to increase tumor uptake by increasing labeled Ab in circulation. This is analogous to the strategy applied for radioimmunotherapy with anti-CD20 Abs (32,33). Furthermore, quantitative imaging of PD-L1 expression pre- and post- administration of anti-PD-L1 Ab therapy could serve to evaluate potential efficacy of the treatment. The reduction of ^{111}In-DTPA-PD-L1 uptake in the tumor environment post-administration of anti-PD-L1 therapy could provide an assessment of the dose delivered to tumors, providing prognostic implications.

These results support future work on the use of PD-L1-targeted molecular imaging agents to help better predict the response to anti-PD-L1 treatment in patients. Quantification of targeted PD-L1 SPECT imaging could help guide clinical trial design by stratifying patients based upon PD-L1 expression in the tumor and tumor microenvironment. In combination, with pharmacokinetic modeling such studies could also help determine the range of Ab doses to be evaluated in a multi-arm trial wherein the mg of Ab administered differs for each arm. Such an approach would introduce a pharmacokinetic level of precision medicine to immune checkpoint therapy (34).

As with other tumor-associated markers, increased expression of PD-L1 on cancer cells and in the tumor microenvironment is both an indicator of a more aggressive cancer phenotype (35,36) and an opportunity to utilize a more effective therapy. In addition, PD-L1 is also expressed on TAMs (8). This observation suggests that the use of anti-PD-L1 Ab for imaging and, particularly for therapy, may have substantial advantages over conventional radionuclide targeting using Ab that only target tumor cells. Radiation delivery that is mediated by anti-PD-L1 Ab may also have some advantages over radiation delivery by an external beam. Depending upon the range and type of radiation emitted by an anti-PD-L1 radioimmunoconjugate, targeted delivery has the potential of killing tumor cells as well as those cells that are most responsible for suppressing anti-tumor immunity while also providing the type of immune modulation observed with external beam radiation therapy (37).

The SPECT imaging and biodistribution studies showed that anti-PD-L1 Ab has a favorable biodistribution for radiopharmaceutical therapy. The dosimetric calculations for the imaging radionuclide ^{111}In and the therapeutic beta-emitting radionuclides ^{177}Lu and ^{90}Y were based on our biodistribution data, which were translated to a human adult male using organ weights from the software, OLINDA/EXM (Table 1). The dosimetric calculations for ^{111}In, ^{177}Lu and ^{90}Y demonstrate that the spleen is expected to receive the highest AD followed by the tumor, liver and thymus. Although the spleen AD is higher than the tumor AD, the spleen is not considered a vital organ, suggesting that the dose-limiting organ will be the red marrow. Almost all antibody-mediated radiopharmaceutical therapy is associated

Author Manuscript Author Manuscript Author Manuscript Author Manuscript

with hematologic toxicity, limiting the dose. The thymus and liver are less of a concern since reduced thymus function is not life threatening and the liver is less sensitive to radiation. The calculated AD is most likely an overestimation for the adult human, due to differences in metabolism and pharmacokinetics compared to a mouse. However, these calculations provide insight into the possible dose-limiting organs for radiotherapeutic anti-PD-L1 Ab conjugates, and also provide preliminary estimates of tumor AD.

Conclusion

The imaging and biodistribution studies presented highlight the importance of PD-L1 targeted imaging in the optimization and monitoring of checkpoint inhibition therapy. These results also suggest an important role for pre-dosing in radiopharmaceutical therapy with anti-PD-L1 antibody. Pre-dosing with unlabeled antibody, in this case would be consistent with a combination treatment strategy, in which targeted radiation complements checkpoint blockade by killing cells involved in inhibiting anti-tumor immunity.

Acknowledgments

We thank Drs. Elizabeth Jaffee and Linda Liu for providing helpful discussions and insight regarding anti-PD-L1 therapy.

Grant support: National Institute of Health grant R01 CA 187037 (G. Sgouros).

References

1. Dong H, Zhu G, Tamada K, Chen L. B7-H1, a third member of the B7 family, co-stimulates T-cell proliferation and interleukin-10 secretion. Nat Med. 1999; 5(12):1365–9. [PubMed: 10581077]
2. Vidal-Laliena M, Romero X, March S, Requena V, Petriz J, Engel P. Characterization of antibodies submitted to the B cell section of the 8th Human Leukocyte Differentiation Antigens Workshop by flow cytometry and immunohistochemistry. Cell Immunol. 2005; 236(1-2):6–16. [PubMed: 16157322]
3. Pardoll DM. The blockade of immune checkpoints in cancer immunotherapy. Nat Rev Cancer. 2012; 12(4):252–64. [PubMed: 22437870]
4. Carter L, Fouser LA, Jussif J, Fitz L, Deng B, Wood CR, et al. PD-1:PD-L inhibitory pathway affects both CD4(+) and CD8(+) T cells and is overcome by IL-2. Eur J Immunol. 2002; 32(3):634–43. [PubMed: 11857337]
5. Brahmer JR, Tykodi SS, Chow LQM, Hwu WJ, Topalian SL, Hwu P, et al. Safety and Activity of Anti–PD-L1 Antibody in Patients with Advanced Cancer. New England Journal of Medicine. 2012; 366(26):2455–65. [PubMed: 22658128]
6. Topalian SL, Hodi FS, Brahmer JR, Gettinger SN, Smith DC, McDermott DF, et al. Safety, Activity, and Immune Correlates of Anti–PD-1 Antibody in Cancer. New England Journal of Medicine. 2012; 366(26):2443–54. [PubMed: 22658127]
7. Emens L, Braiteh F, Cassier P, Delord J, Eder J, Shen X, et al. Inhibition of PD-L1 by MPDL3280A leads to clinical activity in patients with metastatic triple-negative breast cancer. 2014
8. Herbst RS, Soria JC, Kowanetz M, Fine GD, Hamid O, Gordon MS, et al. Predictive correlates of response to the anti-PD-L1 antibody MPDL3280A in cancer patients. Nature. 2014; 515(7528): 563–7. [PubMed: 25428504]
9. Patel SP, Kurzrock R. PD-L1 Expression as a Predictive Biomarker in Cancer Immunotherapy. Mol Cancer Ther. 2015; 14(4):847–56. [PubMed: 25695955]
10. Song H, Shahverdi K, Huso DL, Wang Y, Fox JJ, Hobbs RF, et al. An immunotolerant HER-2/neu transgenic mouse model of metastatic breast cancer. Clin Cancer Res. 2008; 14(19):6116–24. [PubMed: 18829490]

Author Manuscript Author Manuscript Author Manuscript Author Manuscript

11. Strome SE, Dong H, Tamura H, Voss SG, Flies DB, Tamada K, et al. B7-H1 blockade augments adoptive T-cell immunotherapy for squamous cell carcinoma. Cancer research. 2003; 63(19): 6501–05. [PubMed: 14559843]
12. Brechbiel MW, Gansow OA. Synthesis of C-functionalzied trans-cyclohexyldiethylenetriaminepenta-acetic acids for labeling of monoclonal antibodies with bismuth-212 alpha-particle emitter. J Chem Soc Perkin Trans I. 1992; 1:1173–78.
13. Brechbiel MW. Bifunctional chelates for metal nuclides. The Quarterly Journal of Nuclear Medicine and Molecular Imaging. 2008; 52(2):166–73. [PubMed: 18043537]
14. Reilly RT, Gottlieb MBC, Ercolini AM, Machiels JPH, Kane CE, Okoye FI, et al. HER-2/neu is a tumor rejection target in tolerized HER-2/neu transgenic mice. Cancer Research. 2000; 60(13): 3569–76. [PubMed: 10910070]
15. Reilly RT, Machiels JPH, Emens LA, Ercolini AM, Okoye FI, Lei RY, et al. The collaboration of both humoral and cellular HER-2/neu-targeted immune responses is required for the complete eradication of HER-2/neu-expressing tumors. Cancer Research. 2001; 61(3):880–83. [PubMed: 11221874]
16. Hirano F, Kaneko K, Tamura H, Dong H, Wang S, Ichikawa M, et al. Blockade of B7-H1 and PD-1 by Monoclonal Antibodies Potentiates Cancer Therapeutic Immunity. Cancer Research. 2005; 65(3):1089–96. [PubMed: 15705911]
17. Guy CT, Webster MA, Schaller M, Parsons TJ, Cardiff RD, Muller WJ. Expression of the Neu Protooncogene in the Mammary Epithelium of Transgenic Mice Induces Metastatic Disease. Proceedings of the National Academy of Sciences of the United States of America. 1992; 89(22): 10578–82. [PubMed: 1359541]
18. Branderhorst W, Vastenhouw B, Beekman FJ. Pixel-based subsets for rapid multi-pinhole SPECT reconstruction. Phys Med Biol. 2010; 55(7):2023–34. [PubMed: 20299722]
19. Song H, Shahverdi K, Huso DL, Esaias C, Fox J, Liedy A, et al. 213Bi (alpha-emitter)-antibody targeting of breast cancer metastases in the neu-N transgenic mouse model. Cancer Res. 2008; 68(10):3873–80. [PubMed: 18483272]
20. Cristy, M.; Eckerman, KF. Specific absorbed fractions of energy at various ages for internal photon sources. Oak Ridge, TN: Oak Ridge National Laboratory; 1987. Report No. ORNL/TM-8381
21. Snyder, WS.; Cook, MJ.; Nasset, ES.; Karhausen, LR.; Howells, GP.; Tipton, IH. ICRP Publication 23, Report of the task group on reference man. Elmsford, NY: International Commission on Radiological Protection; 1975.
22. Sgouros G. Bone marrow dosimetry for radioimmunotherapy: theoretical considerations. J Nucl Med. 1993; 34(4):689–94. [PubMed: 8455089]
23. Bolch WE, Eckerman KF, Sgouros G, Thomas SR. MIRD pamphlet No. 21: a generalized schema for radiopharmaceutical dosimetry--standardization of nomenclature. J Nucl Med. 2009; 50(3): 477–84. [PubMed: 19258258]
24. Loevinger, R.; Berman, M. MIRD Pamphlet No 1 (revised). New York: The Society of Nuclear Medicine; 1976. A revised schema for calculating the absorbed dose from biologically distributed radionuclides.
25. Stabin MG, Sparks RB, Crowe E. OLINDA/EXM: the second-generation personal computer software for internal dose assessment in nuclear medicine. J Nucl Med. 2005; 46(6):1023–7. [PubMed: 15937315]
26. Deng L, Liang H, Burnette B, Beckett M, Darga T, Weichselbaum RR, et al. Irradiation and anti-PD-L1 treatment synergistically promote antitumor immunity in mice. The Journal of clinical investigation. 2014; 124(2):687–95. [PubMed: 24382348]
27. Zeng J, See AP, Phallen J, Jackson CM, Belcaid Z, Ruzevick J, et al. Anti-PD-1 blockade and stereotactic radiation produce long-term survival in mice with intracranial gliomas. Int J Radiat Oncol Biol Phys. 2013; 86(2):343–9. [PubMed: 23462419]
28. Chen J, Feng Y, Lu L, Wang H, Dai L, Li Y, et al. Interferon-gamma-induced PD-L1 surface expression on human oral squamous carcinoma via PKD2 signal pathway. Immunobiology. 2012; 217(4):385–93. [PubMed: 22204817]

Author Manuscript Author Manuscript Author Manuscript Author Manuscript

29. Furuta J, Inozume T, Harada K, Shimada S. CD271 on melanoma cell is an IFN-gamma-inducible immunosuppressive factor that mediates downregulation of melanoma antigens. J Invest Dermatol. 2014; 134(5):1369–77. [PubMed: 24226422]

30. Liang SC, Latchman YE, Buhlmann JE, Tomczak MF, Horwitz BH, Freeman GJ, et al. Regulation of PD-1, PD-L1, and PD-L2 expression during normal and autoimmune responses. Eur J Immunol. 2003; 33(10):2706–16. [PubMed: 14515254]

31. Heskamp S, Hobo W, Molkenboer-Kuenen JD, Olive D, Oyen WJ, Dolstra H, et al. Noninvasive Imaging of Tumor PD-L1 Expression Using Radiolabeled Anti-PD-L1 Antibodies. Cancer Res. 2015; 75(14):2928–36. [PubMed: 25977331]

32. Buchsbaum DJ, Wahl RL, Glenn SD, Normolle DP, Kaminski MS. Improved delivery of radiolabeled anti-B1 monoclonal antibody to Raji lymphoma xenografts by predosing with unlabeled anti-B1 monoclonal antibody. Cancer Res. 1992; 52(3):637–42. [PubMed: 1732052]

33. Kaminski MS, Zasadny KR, Francis IR, Milik AW, Ross CW, Moon SD, et al. Radioimmunotherapy of B-cell lymphoma with [131I]anti-B1 (anti-CD20) antibody. N Engl J Med. 1993; 329(7):459–65. [PubMed: 7687326]

34. Sgouros G, Goldenberg DM. Radiopharmaceutical therapy in the era of precision medicine. Eur J Cancer. 2014; 50(13):2360–3. [PubMed: 24953565]

35. Mu CY, Huang JA, Chen Y, Chen C, Zhang XG. High expression of PD-L1 in lung cancer may contribute to poor prognosis and tumor cells immune escape through suppressing tumor infiltrating dendritic cells maturation. Med Oncol. 2011; 28(3):682–8. [PubMed: 20373055]

36. Gao Q, Wang XY, Qiu SJ, Yamato I, Sho M, Nakajima Y, et al. Overexpression of PD-L1 significantly associates with tumor aggressiveness and postoperative recurrence in human hepatocellular carcinoma. Clin Cancer Res. 2009; 15(3):971–9. [PubMed: 19188168]

37. Burnette B, Weichselbaum RR. Radiation as an immune modulator. Semin Radiat Oncol. 2013; 23(4):273–80. [PubMed: 24012341]

Author Manuscript Author Manuscript Author Manuscript Author Manuscript

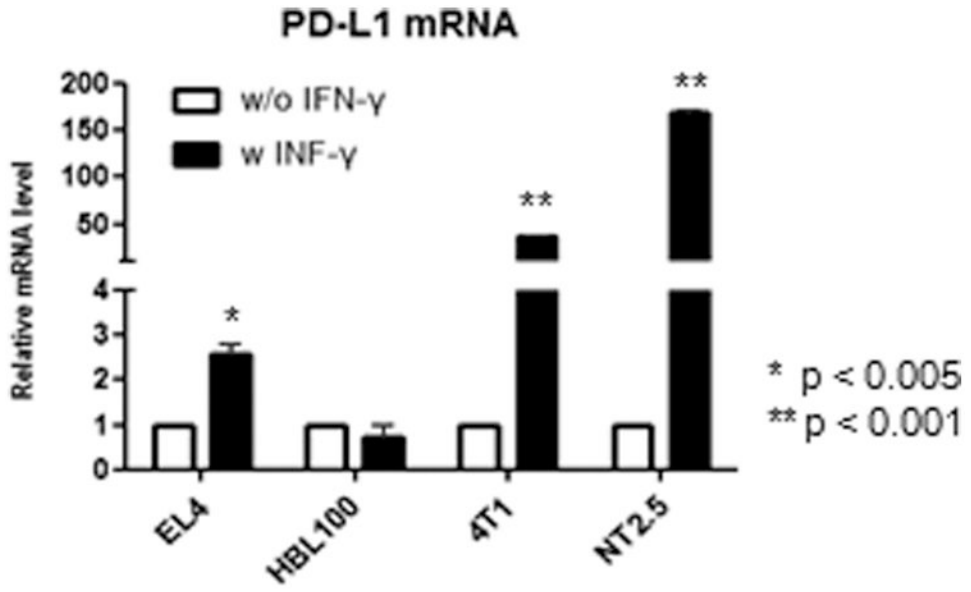

Figure 1.

The real-time RT-qPCR was performed in EL4 (murine B7H1-positive cells), HBL100 (human breast cancer cells), 4T1 (murine breast tumor cells) and NT2.5 (mouse HER2 expressing mammary tumor cell line) cell lines with (w) and without (w/o) 200 ng/ml IFN-γ treatment for 24 hrs. The white bar shows the relative gene expression for the cell line w/o IFN-γ treatment normalized to 1. The black bar shows the relative gene expression of the cell lines with IFN-γ treatment relative the non-treated.

Author Manuscript Author Manuscript Author Manuscript Author Manuscript

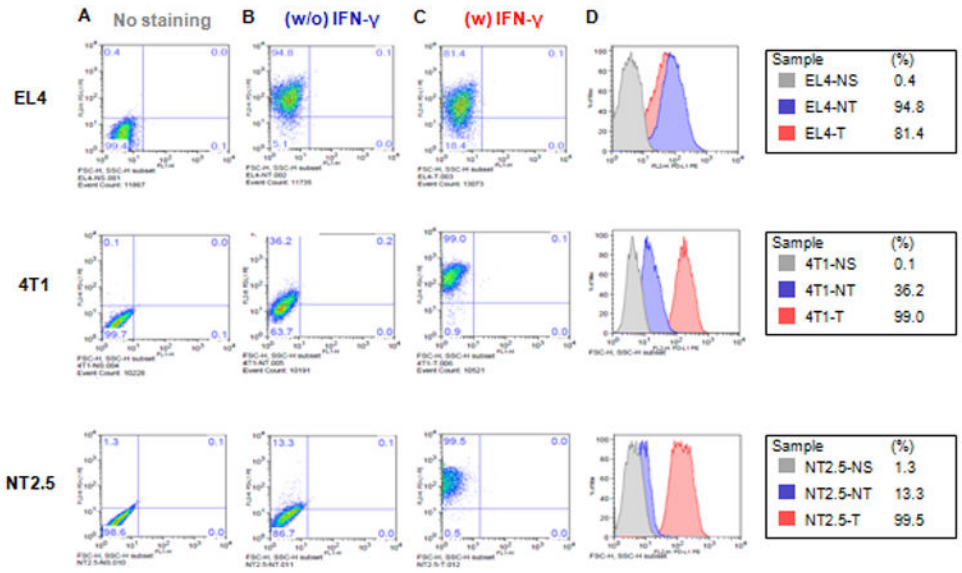

Figure 2.

The flow cytometry for three different cell lines, EL4 (murine B7H1 cells that expresses PD-L1, positive control), 4T1 (murine breast tumor cells) and NT2.5 (mouse HER2 expressing mammary tumor cell line) with **A:** No staining with anti-PD-L1 Ab **B:** Staining with anti-PD-L1 Ab and without (w/o) INF-γ treatment and **C:** Staining with anti-PD-L1 Ab and treatment with (w) 200 ng/ml IFN-γ for 24 hrs. **D:** Shows the shift for no staining (NS, grey), staining with anti-PD-L1 Ab w/o INF-γ treatment (NT, blue), and staining with anti-PD-L1 Ab with INF-γ treatment (T, red).

Author Manuscript Author Manuscript Author Manuscript Author Manuscript

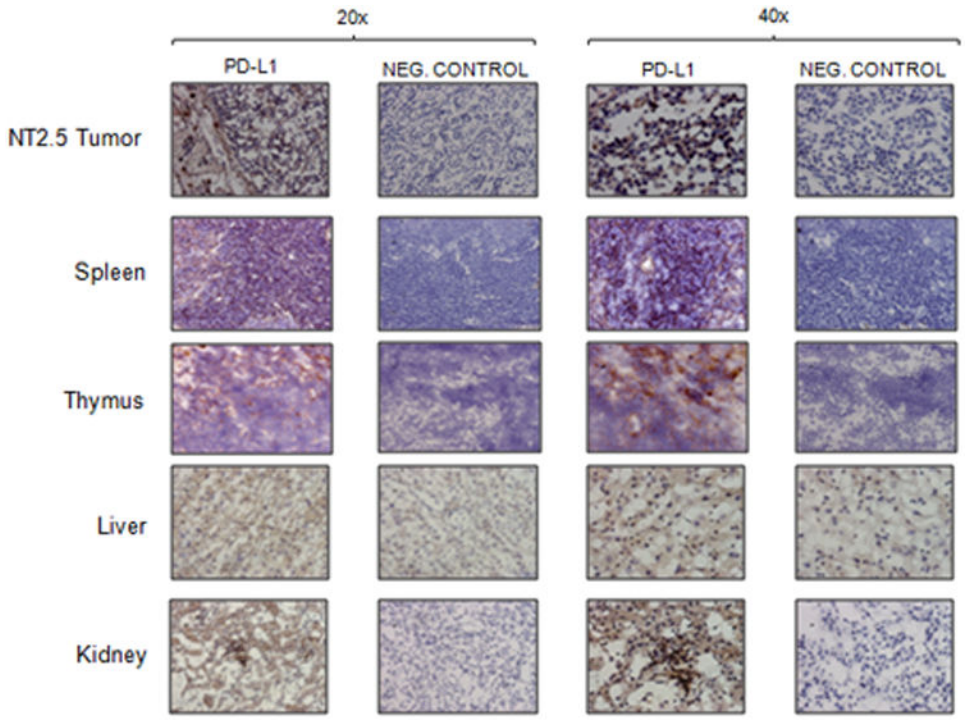

Figure 3.

Immunohistochemistry of PD-L1 expression (PD-L1) and negative control (NEG. CONTROL) for NT2.5 tumor, spleen, thymus, liver and kidney at 20× and 40× magnification.

Author Manuscript Author Manuscript Author Manuscript Author Manuscript

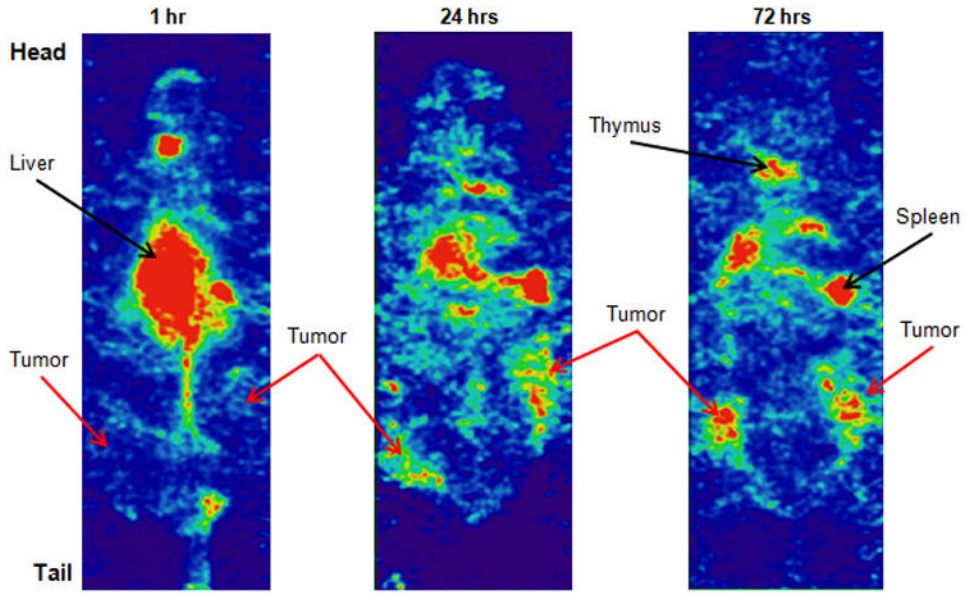

Figure 4.

Whole-body SPECT images (coronal view) in transgenic *neu*-N mice showing the uptake in normal tissues (e.g. spleen, thymus and liver) and tumors for anti-PD-L1 Ab labeled with ^{111}In at 1, 24 and 72 hrs p.i.

Author Manuscript Author Manuscript Author Manuscript Author Manuscript

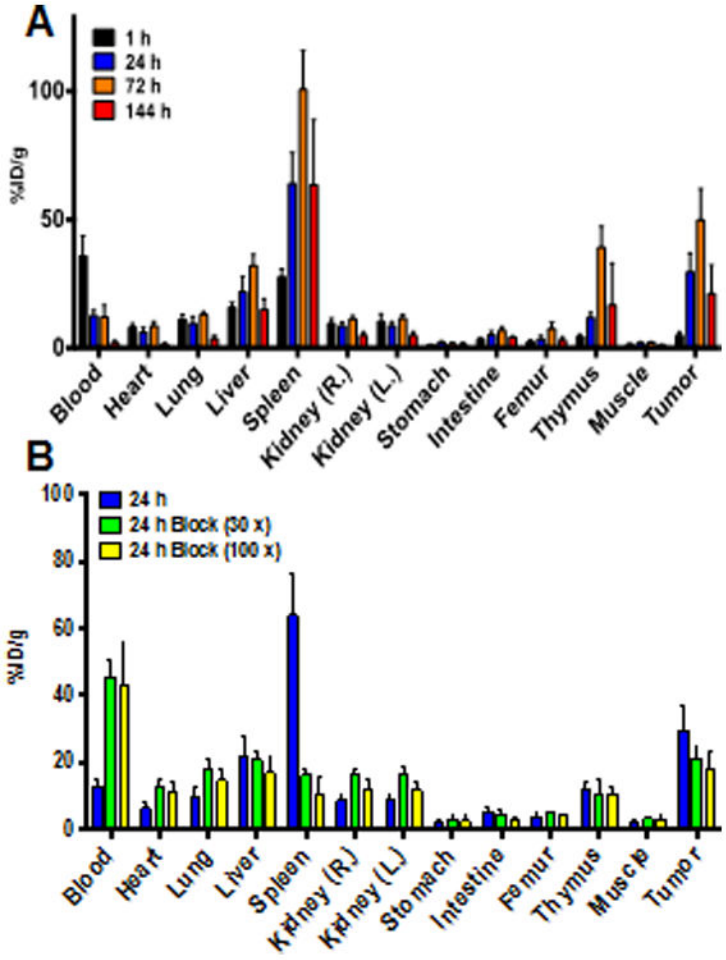

Figure 5.

A: Biodistribution in tumor bearing transgenic *neu*-N mice for the normal tissues blood, heart, lung, liver, kidneys, stomach (with content), intestine (with content), femur, thymus, muscle and tumor for anti-PD-L1 Ab at 1 h (black bar), 24 hrs (blue bar), 72 hrs (orange bar), and 144 hrs (red bar) p.i. **B:** Biodistribution in *neu*-N mice at 24 hrs p.i. for normal tissues and tumor of anti-PD-L1 Abs (blue bar) and co-injected for blocking with excess cold anti-PD-L1 Ab 30× (green bar) and 100× (yellow bar).

Author Manuscript

Author Manuscript

Author Manuscript

Author Manuscript

Table 1

Dosimetric calculations expressed in mGy per injected MBq for the spleen, liver, thymus, kidneys, red marrow and tumor for anti-PD-L1 antibodies labeled with the therapeutic beta particle emitters ^{177}Lu and ^{90}Y, and the diagnostic imaging radionuclide ^{111}In. The absorbed dose calculated for normal tissues and tumors were based on *neu*-N mouse biodistribution data, which were converted into adult human ADs. The calculated time integrated activities were used as input in OLINDA/EXM using the adult male phantom for normal tissues, and using the sphere model to calculate the absorbed dose for the tumor.

	^{177}Lu-anti-PD-L1	***^{90}Y-anti-PD-L1***	***^{111}In-anti-PD-L1***
Tissue	**Absorbed dose (mGy/MBq)**	**Absorbed dose (mGy/MBq)**	**Absorbed dose(mGy/MBq)**
Spleen	2.5	8.2	0.7
Liver	0.8	2.7	0.3
Thymus	0.7	2.2	0.1
Kidneys	0.3	1.1	0.1
Red marrow	0.1	0.3	0.02
Tumor	1.1	3.0	0.2